

# Journal Pre-proof

Protein encapsulation in functionalized sol-gel silica: Effect of the encapsulation method on the release kinetics and the activity

Rémi G. Tilkin, Xavier Colle, Anthony Argento Finol, Nicolas Régibeau, Julien G. Mahy, Christian Grandfils, Stéphanie D. Lambert



PII: S1387-1811(20)30504-7

DOI: <https://doi.org/10.1016/j.micromeso.2020.110502>

Reference: MICMAT 110502

To appear in: *Microporous and Mesoporous Materials*

Received Date: 13 December 2019

Revised Date: 27 May 2020

Accepted Date: 14 July 2020

Please cite this article as: Ré.G. Tilkin, X. Colle, A.A. Finol, N. Régibeau, J.G. Mahy, C. Grandfils, Sté.D. Lambert, Protein encapsulation in functionalized sol-gel silica: Effect of the encapsulation method on the release kinetics and the activity, *Microporous and Mesoporous Materials* (2020), doi: <https://doi.org/10.1016/j.micromeso.2020.110502>.

This is a PDF file of an article that has undergone enhancements after acceptance, such as the addition of a cover page and metadata, and formatting for readability, but it is not yet the definitive version of record. This version will undergo additional copyediting, typesetting and review before it is published in its final form, but we are providing this version to give early visibility of the article. Please note that, during the production process, errors may be discovered which could affect the content, and all legal disclaimers that apply to the journal pertain.

© 2020 Published by Elsevier Inc.

*CRedit author statement*

Rémi G. Tilkin: Conceptualization, Methodology, Validation, Formal analysis, Investigation, Data Curation, Writing - Original Draft, Writing - Review & Editing, Visualization, Funding acquisition.

Xavier Colle: Conceptualization, Methodology, Formal analysis, Investigation.

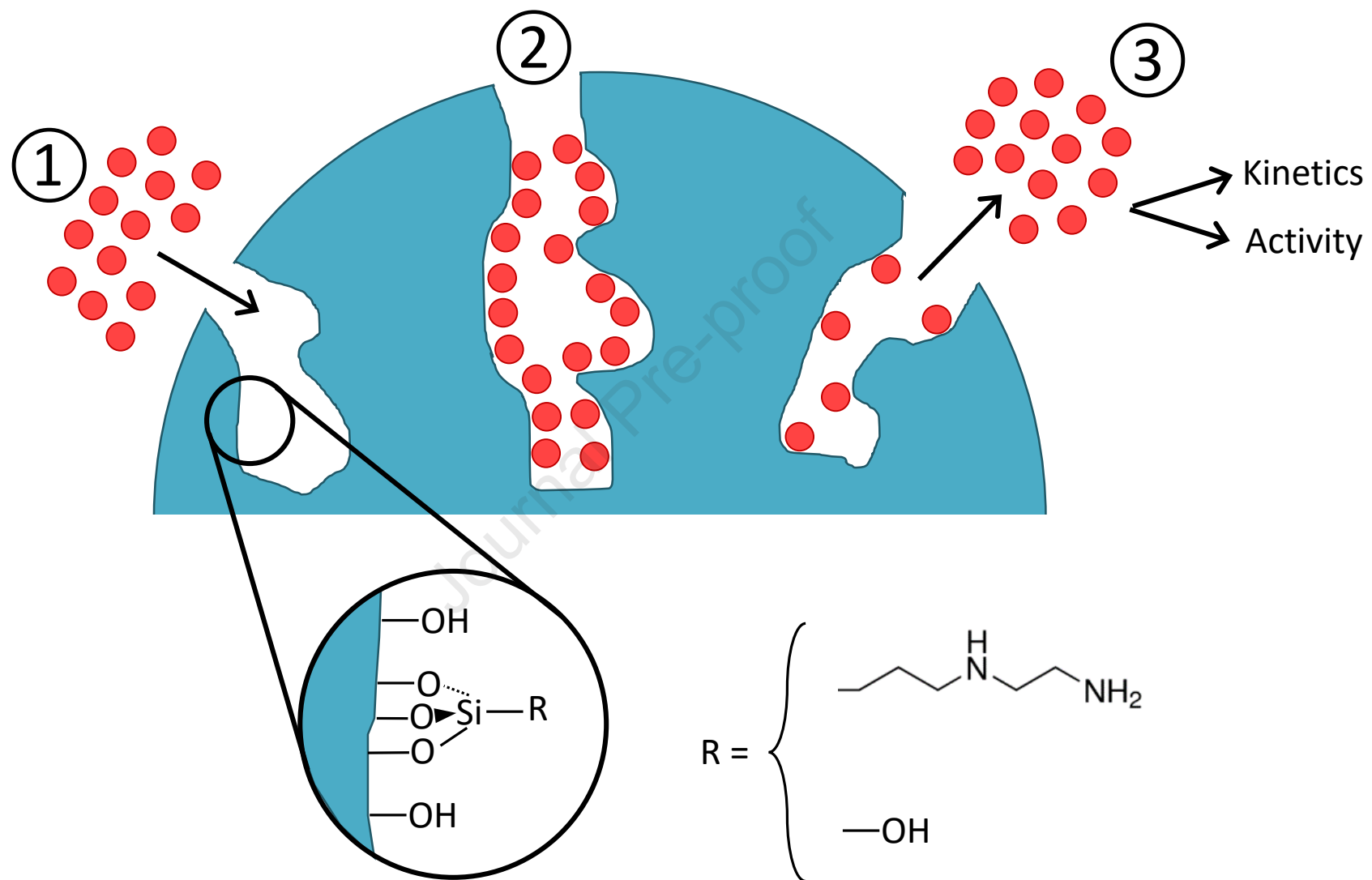
Anthony Argento Finol: Methodology, Investigation.

Nicolas Régibeau: Validation, Writing - Review & Editing.

Julien G. Mahy: Validation, Formal analysis, Writing - Review & Editing.

Christian Grandfils: Conceptualization, Resources, Writing - Review & Editing, Supervision, Project administration.

Stéphanie D. Lambert: Conceptualization, Resources, Writing - Review & Editing, Supervision, Project administration.



# Protein encapsulation in functionalized sol-gel silica: effect of the encapsulation method on the release kinetics and the activity

*Rémi G. Tilkin<sup>\*a,b</sup>, Xavier Colle<sup>a,b</sup>, Anthony Argento Finol<sup>b</sup>, Nicolas Régibeau<sup>a,b</sup>, Julien G. Mahy<sup>c</sup>, Christian Grandfils<sup>b</sup>, Stéphanie D. Lambert<sup>a</sup>*

<sup>a</sup> Department of Chemical Engineering – Nanomaterials, Catalysis and Electrochemistry (NCE), University of Liège, Allée du Six Août 11, 4000 Liège, Belgium

<sup>b</sup> Interfaculty Research Center of Biomaterials (CEIB), University of Liège, Allée du Six Août 11, 4000 Liège, Belgium

<sup>c</sup> Institute of Condensed Matter and Nanosciences (IMCN), Université catholique de Louvain, Place Louis Pasteur 1, 1348, Louvain-la-Neuve, Belgium

Corresponding author: Rémi G. Tilkin; email: rtilkin@uliege.be ; address: Allée du Six Août 11, 4000 Liège, Belgium

## ABSTRACT

Over the last few years, bone repair has increasingly gained in importance. In recent years, considerable attention has been given to the administration of therapeutic biomolecules to promote tissue regeneration. The aim of this work is the study of the influence of functional groups present at the surface of silica pores and the textural structure on the release kinetics of a model protein (*i.e.* Soybean Trypsin Inhibitor, STI) and on the preservation of its inhibitory activity. For this purpose, two alternative methods have been investigated: i) impregnation of presynthesized silica gels with the protein solution (*i.e.* impregnation method), ii) direct incorporation of the protein during the synthesis of the gel (*i.e.* *in situ* method). Regarding the impregnation method, a fast release of STI was observed when incubated in physiological conditions (*i.e.* burst followed by a plateau for the calcined samples or by a sustained release for the dried sample) while the *in situ* method allowed a better control of the release rate of this protein over the first 24 h. This difference in release kinetics could be explained in terms of the expected geometry of the pores (open versus closed porosity). Interestingly, no significant change in the activity of the protein was noticed for the silica synthesized via the *in situ* method, while a partial or total loss of inhibitory activity was measured after four weeks of incubation for the impregnated silica.

Keywords: biomaterials, bone reconstruction, protein encapsulation, silica gel, sol-gel process, surface modification.

## 1. INTRODUCTION

Bone possesses the capacity of self-regeneration allowing its repair without any scar [1,2]. However, in the case of large fracture defects (*i.e.* gaps beyond two and a half times the bone radius), this physiological repair is not sufficient and requires external assistance in order to recover the complete structure and function of the native bone [3]. Every year, over 4 million surgical procedures involving bone grafting or bone graft substitutes are performed worldwide, making bones the second most grafted organ after blood transfusion [4,5]. Moreover, the importance of bone repair is expected to increase within the next decades with the aging of the population (*i.e.* almost doubling of the population over 65 years in 2050) and the constant increase in implementation of healthcare services worldwide [6].

Several materials have been developed to promote bone healing [7–10]. In recent years, considerable attention has been given to the administration of therapeutic biomolecules to promote tissue regeneration [11,12]. In particular, bone morphogenetic proteins (BMP), a family of cytokines, are well-known to be good candidate to promote bone reconstruction [13–15]. Indeed, BMPs have been shown to induce significant bone formation via the regulation of cell adhesion, proliferation, differentiation, and apoptosis in bone tissue. Studies have showed that BMP-2 could promote the bone differentiation of stem cells as well as the fracture repair through the recruitment of osteogenic progenitor cells [16–18]. Moreover, BMP-2 and BMP-7 have been approved by the Food and Drug Administration for the treatment of bone fractures [13,19]. To achieve a good reconstruction process, the release of BMP from the matrix must be controlled to avoid undesirable growth of tumors or neovascularization of non-targeted tissues due to an excessively high dose of growth factors [20]. Several delivery system have already been proposed for the sustained delivery of BMP [21–23]. Among them, silica gels have gained increasing interest to control the sustained release of different biomolecules in tissue engineering

[24–29]. Sol-gel silica is an amorphous porous material formed by an interconnected network of silicon atoms, which can be synthesized under soft conditions not detrimental to the activity of these biomolecules (*e.g.* via sol-gel process) [30–33]. One of the most attractive features of this material is its large specific surface area, allowing a large amount of biomolecules to be adsorbed at the surface of the pores [34]. Moreover, the morphology of the pores can be tuned with the synthesis conditions (*e.g.* *pH*, solvent, processing conditions) in order to match the hydrodynamic diameter of typical biomolecules and to regulate the diffusion inside the pores and the subsequent release process [24,33,35]. The surface chemistry of the wall of the pores can also be modified to graft functional groups allowing the adjustment of their surface charge density or their hydrophilic/hydrophobic balance to modulate the interaction (*i.e.* electrostatic forces, hydrogen bonding, van der Waals forces) between the protein and the pore walls [35–38]. From a processing perspective, silica gels can be processed in a wide variety of forms ranging from monoliths to films and particles (micro and nano size) [24,30,36]. Silica is also very interesting from a biocompatible point of view, being resorbable and non-toxic [30,34,39]. Furthermore, studies have shown that immobilization of enzymes protects them against physico-chemical stresses that could alter their structural integrity and their biological activity [26]. This inorganic material also offers as additional advantages, limited swelling and good mechanical stability [25,40].

In this study, a model protein has been chosen: the Soybean Trypsin Inhibitor (STI). STI has been chosen because of its similarities with BMP in term of size, molecular weight, point of zero charge, hydrophobic properties, and release kinetics (see Table 1).[30,41,42]. This protein has been used in previous studies to model BMP release [7,30,42]. The encapsulation of BMP and STI inside silica gels has already been studied through the impregnation of pre-synthesized gels (*i.e.* impregnation method) [12,43–45] and the direct incorporation of protein during the

formation of the gel (*i.e. in situ* method) [7,30,46,47]. Due to the versatility of the sol-gel method, silica gels have been processed to produce different forms such as particles [7,12,46,47], films [20,30,43,44], and complete scaffolds [45]. These studies have showed that immobilization of these proteins in silica and their subsequent release over several days and even weeks is feasible. However, even if the materials were characterized in terms of composition and porosity, these studies did not directly present the link between the textural properties and surface chemistry of silica, and the release kinetics and remaining activity of the proteins. Indeed, the textural properties and the surface chemistry of silica play a key role in these phenomena by greatly influencing the diffusion of the proteins inside the pores. They also modulate the protein activity via interactions with the functional groups present at the pore surface or by physical restriction of the protein conformation [35,36]. Altering the textural properties (*e.g.* pore size, surface area) as well as the surface chemistry (*e.g.* addition of specific functional groups) would thus be of great interest. Moreover, the complete comparison of the different encapsulation methods (mainly, impregnation and *in situ* method) has not been realized, even though they provide different features with their own advantages and drawbacks.

Based on this rational, the aim of this work was the study of the influence of the textural properties and surface chemistry on the encapsulation of proteins in functionalized silica gels. With this goal, STI has been encapsulated either by impregnation or by *in situ* synthesis. Surface chemistry and textural properties have been controlled via the choice of the method, the use of a nucleating agent for silica particles, and the calcination treatment. These new materials were then characterized via infrared spectroscopy (FTIR) to study the chemical composition, thermogravimetric analysis (TGA) to determine the organic content, nitrogen adsorption-desorption and mercury porosimetry to assess the textural properties, and by the method of equilibrium *pH* at high loading to determine the point of zero charge (PZC). The release kinetics



of the protein *in vitro* as well as the inhibitory activity after release were also determined over a period of 12 weeks.

## 2. MATERIALS AND METHODS

### 2.1. Materials

In this section, the activity of the proteins is expressed in N $\alpha$ -Benzoyl-L-arginine ethyl ester hydrochloride (BAEE) units. In this context, one BAEE unit yields a difference of absorbance at 253 nm ( $\Delta A_{253}$ ) of 0.001/min with BAEE as substrate at  $pH = 7.6$  at 25 °C.

Tetraethyl orthosilicate (TEOS, Si(OC<sub>2</sub>H<sub>5</sub>)<sub>4</sub>), ammonium hydroxide solution NH<sub>3</sub> (28-30 %), 3-(2-aminoethylamino) propyltrimethoxysilane (EDAS, (CH<sub>3</sub>O)<sub>3</sub>Si(CH<sub>2</sub>)<sub>3</sub>NHCH<sub>2</sub>CH<sub>2</sub>NH<sub>2</sub> (97 %)), potassium phosphate monobasic (KH<sub>2</sub>PO<sub>4</sub>), sodium chloride (NaCl), potassium chloride (KCl), and Trypsin from bovine pancreas (Type I, 10,000 BAEE units/mg) were purchased from Sigma-Aldrich ; absolute ethanol (C<sub>2</sub>H<sub>5</sub>OH), hydrochloric acid (HCl (37 %)), and sodium hydroxide (NaOH) from Merck; tetramethyl orthosilicate (TMOS, Si(OCH<sub>3</sub>)<sub>4</sub>), sodium phosphate dibasic (Na<sub>2</sub>HPO<sub>4</sub>), and N $\alpha$ -Benzoyl-L-arginine ethyl ester hydrochloride (BAEE, C<sub>15</sub>H<sub>22</sub>N<sub>4</sub>O<sub>3</sub>·HCl) from Acros Organics; Soybean Trypsin Inhibitor STI ( $\geq 7000$  BAEE units/mg) from Carl Roth. Unless indicated otherwise, all these chemicals were  $\geq 99$  % pure and were used without further purification. Phosphate Buffer Saline (PBS) solution was prepared using 1.4 mM KH<sub>2</sub>PO<sub>4</sub>, 10 mM Na<sub>2</sub>HPO<sub>4</sub>, 137 mM NaCl and 2.7 mM KCl and was adjusted to  $pH = 7.4$  using 0.1 M HCl or 0.1 M NaOH.

### 2.2. Sample preparation

Two processes were used in this study for the encapsulation of STI in silica gels: an impregnation method (denoted Imp) and an *in situ* method (denoted IS).

### 2.2.1 Impregnation method

This procedure was adapted from Lambert *et al.* and Mahy *et al.* [33,48]. The samples were synthesized in absolute ethanol, with TEOS, EDAS, and 0.18 M of aqueous  $\text{NH}_3$  solution. Synthesis processing variables were selected in order to adopt a hydrolysis ratio (*i.e.*  $[\text{H}_2\text{O}] / ([\text{TEOS}] + 3/4 [\text{EDAS}])$ ) equal to 5, a dilution ratio (*i.e.*  $[\text{C}_2\text{H}_5\text{OH}] / ([\text{TEOS}] + [\text{EDAS}])$ ) equal to 10, and a ratio of EDAS to TEOS (*i.e.*  $[\text{EDAS}]/[\text{TEOS}]$ ) equal to 0.2. This gave a molar ratio TEOS : EDAS : ethanol : water :  $\text{NH}_3$  of 157 : 31.5 : 1890 : 903 : 2.9.

The samples were synthesized in absolute ethanol, with TEOS, EDAS, and 0.18 M aqueous  $\text{NH}_3$  solution [33,48]. TEOS (32.71 g) was first mixed with ethanol (55 mL) at room temperature under stirring. EDAS (7 g) was then added under constant agitation. Ethanolic  $\text{NH}_3$  solution (16.3 mL of 0.18 M aqueous  $\text{NH}_3$  solution in 55 mL of ethanol) was finally added to the mixture under vigorous stirring. The volume of the final solutions was about 200 mL. For gelation and ageing, the sample vessel was closed and heated to 80°C for 72 h. Then, the resulting gels were dried under air at room temperature for 72 h. The gels were further dried under vacuum by placing the open vessel in an oven at 150°C at 50 Pa for 24 h. Samples were finally calcined by heating up to 450°C at a rate of 2°C/min for 12 h and then at 550°C for 12 h at a rate of 2°C/min. Imp-Dry sample was obtained after drying, Imp-450 after calcination at 450°C, and Imp-550 after calcination at 550°C.

After the synthesis, the samples were ground and the powder fraction between 300 and 700  $\mu\text{m}$  was kept for further treatments and characterization. This fraction was impregnated in a STI solution (1 mg/mL in PBS) for 3 h or 72 h (50 mg of sample per mL of solution) at 25°C under agitation. The impregnation was undertaken in duplicates. The suspensions were then centrifuged

at 3000 rpm for 5 min and the supernatant was removed. The particles were finally freeze-dried for 3 days. The resulting samples were stored at -20°C.

### 2.2.2. *In situ* method

This procedure was adapted from Reiner *et al.* [30]. The samples were synthesized in PBS, with TMOS, and 2.5 mM of aqueous HCl solution. Synthesis processing variables were selected to ensure a prehydrolysis ratio (*i.e.*  $[\text{H}_2\text{O}]_{\text{prehydrolysis}} / [\text{TMOS}]$ ) equal to 1.25 and a total dilution ratio (*i.e.*  $([\text{H}_2\text{O}]_{\text{prehydrolysis}} + [\text{H}_2\text{O}]_{\text{PBS}}) / [\text{TMOS}]$ ) equal to 19. This gave a molar ratio TMOS : water : HCl of 50.4 : 972.2 :  $2.88 \times 10^{-3}$ .

TMOS (7.67 g) was first prehydrolyzed in dilute aqueous HCl solution (1.15 mL, 2.5 mM) at room temperature for 30 min under constant stirring. STI solution (16.35 mL, 1 mg/mL in PBS) was then added under agitation. For gelation and ageing, the sample vessel was sealed and left at room temperature for 72 h. The gels were finally dried under air at room temperature for 72 h. After the synthesis, the samples were ground into powders and the fraction between 300 and 700  $\mu\text{m}$  was kept for further treatments and characterization. The resulting samples were stored at -20°C. Protein-free gels were prepared for characterization by replacing the protein solution by a protein-free PBS solution. These samples are denoted IS-Blank.

## 2.3. Sample characterization

### 2.3.1. Chemical and physical characterization

The presence of specific functional groups was confirmed by Fourier transformed infrared (FTIR) spectroscopy in ATR mode using an IRAffinity-1 from Shimadzu. The following instrumental settings were used: absorbance, range from 4000 to 400  $\text{cm}^{-1}$ , 30 scans, resolution 2

$\text{cm}^{-1}$ . The spectra were normalized to the peak corresponding to Si-O-Si stretching (around 1050-1060  $\text{cm}^{-1}$ ).

The organic content was determined by thermogravimetric analysis (TGA, TGA 7 from Perkin-Elmer) under nitrogen atmosphere at a heating rate of 20°C/min between 50°C and 90°C and 10°C/min between 90°C and 750°C. The weight loss was measured between 150°C and 750°C.

The textural properties were characterized by nitrogen adsorption-desorption isotherms in an ASAP 2420 multi-sampler adsorption-desorption volumetric device from Micromeritics. From these isotherms, the microporous volume ( $V_{\text{DR}}$ ) and the equivalent microporous surface ( $S_{\text{DR}}$ ) were calculated using Dubinin-Radushkevich theory [49]. The surface area was evaluated using Brunauer, Emmett, and Teller theory ( $S_{\text{BET}}$ ) [49,50]. The mesoporous volume and surface were determined by Barrett, Joyner, and Halenda theory ( $V_{\text{BJH}}$  and  $S_{\text{BJH}}$ ) [50]. The textural properties were also analyzed by mercury porosimetry. The measurements were performed with sample powders from 0.01 to 200 MPa using a Carlo Erba Porosimeter 2000 after a 2-h outgassing at ambient temperature. Analysis of mercury porosimetry was based on Washburn's intrusion theory [50] and on the collapse theory introduced by Pirard *et al.* [51]. The collapse theory was used for samples with aerogel-like texture, which were crushed and not intruded by mercury. Mercury porosimetry measurements provided the specific macroporous volume ( $V_{\text{Hg}}$ ), the buckling model constant ( $k$ ), and the pressure of change from collapse to intrusion ( $P_{\text{I}}$ ) [51]. The combination of nitrogen adsorption-desorption isotherms and mercury porosimetry was used to calculate the pore size distribution [33].

The point of zero charge (PZC) was determined by the method of equilibrium  $pH$  at high loading [52]. The mass of the samples was first adjusted to obtain a surface loading equal to 10,000  $\text{m}^2/\text{L}$

in 20 mL (in line with previous studies [52,53]). The porous solids were then soaked for 3 h under stirring in 20 mL of water solutions of various starting *pH* ranging from 1 to 13 adjusted using HCl or NaOH solutions. After equilibration, the equilibrium *pH* was measured using an InLab Expert Pro-ISM electrode from Mettler Toledo. The PZC of the solid corresponds to a plateau in a plot of the final *pH* vs. the initial *pH* [52].

### 2.3.2. Biochemical characterization

For the impregnation method, the amount of encapsulated proteins was evaluated by measuring the STI concentration remaining in the supernatant after 3 h or 72 h of incubation via the Lowry method using STI as standard (UV-Vis absorbance measurement at 750 nm, spectrophotometer Lambda 25 from Perkin Elmer) [54]. For the *in situ* method, it was assumed that the entire quantity of the protein was encapsulated inside or at the surface of the silica. Hence, the amount of encapsulated proteins was calculated from the amount of sample produced and the amount of STI added during the synthesis.

The kinetics of protein release was determined by immersing 0.1 g of sample in 2.5 mL of PBS solution in closed vials. This analysis was performed in duplicates. Gels were incubated at 37°C under continuously agitation in a water bath. At scheduled times (*i.e.* 30 min, 4 h, 1 day, 1 week, 2 weeks, 4 weeks, 12 weeks), samples were centrifuged at 1000 rpm for 5 min. The supernatant supernatant was removed, stored at -20°C until analysis, and replaced by fresh PBS. The STI concentration was assessed via the Lowry method using STI as standard (UV-Vis absorbance measurement at 750 nm, Lambda 25 spectrophotometer from Perkin Elmer) [54]. For the impregnation method, the kinetics of protein release was determined for samples after 72 h of impregnation.

This technique was adapted from Merck's protocol [55]. The biochemical activity of STI after release was assessed by measuring the reduction of synthetic BAEE. Briefly, 1 mL of protein sample was mixed with 0.25 mL of trypsin solution (1 mg/L trypsin in 1 mM HCl) and 3.75 mL of 1 mM HCl and incubated for 5 min at room temperature. An aliquot (0.1 mL) of this solution was then added to a solution of BAEE (3 mL, 0.25 mM in 1.67 mM Sodium Phosphate Buffer) and HCl (0.1 mL, 1 mM). The increase in absorbance at 253 nm with time was measured at 30°C using a Specord50 Plus spectrophotometer from Analytikjena. The concentration of active protein was calculated using a standard curve obtained using free STI under the same conditions. Finally, the remaining activity was defined as the ratio between the concentration of active proteins and the total concentration of proteins. The analysis of the activity was measured in duplicates for each sample. Sample times of 30 min, 1 week, and 4 weeks after incubation were adopted for the impregnation method and were limited to 1 week of incubation for the *in situ* method due to the low amount of protein released. For the impregnation method, the biochemical activity of STI after release was only determined for samples after 72 h of impregnation.

### 3. RESULTS AND DISCUSSION

#### 3.1. Composition of samples

The characteristic peaks of silica are identified in the FTIR spectra (Figure 1). The peaks corresponding to the bending mode of Si-O-Si groups are observed at 440-444  $\text{cm}^{-1}$  [56–58]. The stretching modes of Si-O-Si groups are detected at 810 (*i.e.* symmetric stretching), 1054 (*i.e.* transverse optical mode of antisymmetric stretching), and 1120-1300  $\text{cm}^{-1}$  (*i.e.* longitudinal optical mode of antisymmetric stretching) for the Imp-450 and Imp-550 samples [57–60]. These values are shifted towards lower wavenumbers for the Imp-Dry sample (*i.e.* 792, 1044, and 1100-1250  $\text{cm}^{-1}$  respectively, for the symmetric, transverse optical mode of antisymmetric, and

longitudinal optical mode of antisymmetric stretching). This shift is related to the deformation of the network to incorporate the organic groups within the silica matrix (*i.e.* greater Si-O-Si angles and Si-O bond lengths) [59]. For the IS sample, the values are 797, 1060, and 1120-1300  $\text{cm}^{-1}$  respectively. Characteristics peaks of silanol groups are found at 560-567  $\text{cm}^{-1}$  (*i.e.* rocking mode of Si-OH groups) and around 900-990 (*i.e.* antisymmetric stretching of Si-OH groups) [56,58–60]. These bands are less marked in the case of the Imp-450 and Imp-550 samples compared to the Imp-Dry sample. This can be explained by the condensation of adjacent silanols into siloxane bonds during the calcination [61,62]. Comparing the two encapsulation methods, a larger proportion of silanols groups can be observed for the *in situ* method. This is probably due to the absence of any thermal treatment (synthesis and drying at room temperature) in the case of the IS sample. The difference in intensity observed for the peaks corresponding to –OH groups (*i.e.* bending at 1635-1645  $\text{cm}^{-1}$  and stretching around 3000-3600  $\text{cm}^{-1}$ ) follows the same explanations. The presence of –NH-(CH<sub>2</sub>)<sub>2</sub>-NH<sub>2</sub> groups is revealed in Imp-Dry by the presence of peaks corresponding to –CH groups (*i.e.* bending at 691 and 1412  $\text{cm}^{-1}$ ), –CH<sub>2</sub> groups (*i.e.* bending at 1365  $\text{cm}^{-1}$  and 1459  $\text{cm}^{-1}$  and stretching around 2800-3000  $\text{cm}^{-1}$ ), and –NH<sub>2</sub> groups (*i.e.* bending at 1600  $\text{cm}^{-1}$ ) [59,63,64]. After calcination at 450°C, most of these organic groups are replaced by –OH groups (*i.e.* bending at 1645  $\text{cm}^{-1}$  and stretching around 3600  $\text{cm}^{-1}$ ) but some organic groups are still present (*i.e.* bending of –CH<sub>2</sub> groups at 1366  $\text{cm}^{-1}$ ) probably due to an incomplete combustion [56–59,63]. After calcination at 550°C, only –OH groups are detected (*i.e.* –OH stretching around 3000-3600  $\text{cm}^{-1}$ ) [56–59]. Regarding the IS sample, only characteristic peaks of silica and –OH groups are observed.

The percentage of organic content of the functionalized silica samples was determined by TGA (Table 2). In the case of the impregnation method, it is observed that the organic content depends

on the thermal post treatment. Imp-Dry sample presents a large weight decrease due to the presence of ethylene diamine groups at the surface of the pores. This amount is similar to the theoretical organic content of 22.7 wt% and corresponds to a concentration of 2.05 mmol/g.

Calcined samples exhibit a much lower organic content compared to the dried sample because of the combustion of ethylene diamine groups during the calcination step. Nevertheless, a weight decrease is measured, which correspond to the condensation of adjacent silanols at high temperature with the formation of siloxane bonds and the release of water molecules [61,62]. The proportion of uncondensed silanols decreases with the calcination temperature, leading to a slightly smaller weight decrease for Imp-550 sample compared to Imp-450 sample. These observations are in concordance with the conclusions made regarding FTIR spectra. The weight decrease observed in the case of the IS sample can also be explained by the condensation of silanols. The values observed respectively for the Imp-450, Imp-550, and IS samples correspond to a concentration of 4.6, 4.5, and 4.9 –OH groups/nm<sup>2</sup> respectively, which is in agreement with those obtained by Zhuravlev *et al.*[65].

### 3.2. Textural properties analysis

To adjust the release kinetics and protect the protein from denaturation, the textural properties are important parameters to consider because of their key role regarding protein diffusion and physical interaction between the protein and the matrix. A compromise needs to be identified in the mean pore size of silica. A reduction of their size will increase the surface area accessible for protein adsorption, but will also limit their accessibility and the diffusion rate of the biomolecules afterwards [34,35]. As already mentioned, the pore morphology can be controlled during the synthesis notably through the *pH*, the temperature or the solvent, and is controlled in an easier



way in the case of the impregnation method [32,66]. On the other hand, physical and geometrical interactions between the pore walls and the proteins can also regulate the diffusion inside the pores and consequently the release kinetics.

The nitrogen adsorption-desorption isotherms are depicted in Figure 2(a). The textural properties of the samples are given in Table 3. Two types of isotherms are present depending on the synthesis method. For the impregnation method, a mixture of Types I and IV isotherms according to the BDDT classification are observed [49]. They are characterized by a rapid increase of the adsorbed volume at low pressure due to the micropore filling as in Type I isotherm (microporous solid) and by the presence of a hysteresis resulting from capillary condensation as in Type IV isotherm (mesoporous solid). The hysteresis presents a H2 Type shape [67]. The steep desorption branch is due to pore-blocking resulting from the presence of large mesopores with narrow mouths (*i.e.* bottle-like pores). This is also confirmed by the BJH distribution (*i.e.* presence of a small peak at 8.8, 9.4, and 8.9 nm for Imp-Dry, Imp-450, and Imp-550 samples respectively and a larger peak at 18.7, 19.0, and 18.4 nm respectively) and the higher value of the mesoporous volume  $V_{\text{BJH}}$  compared to the total pore volume,  $V_{\text{T}}$  (representative for meso and macroporous solids). The lower surface area of Imp-Dry sample (*i.e.* 330 m<sup>2</sup>/g) is explained by the presence of the ethylene diamine groups inside the pores. These groups are degraded after calcination at 450°C, which increases the surface area of Imp-450 sample (*i.e.* 585 m<sup>2</sup>/g) compared to Imp-Dry sample. At 550°C, the silica sintering process occurs, which leads to a reduction of the specific surface area of Imp-550 sample (*i.e.* 445 m<sup>2</sup>/g) [32]. These values are in concordance with previous studies [33,68]. The higher  $V_{\text{DR}}$ ,  $V_{\text{BJH}}$ , and  $S_{\text{BJH}}$  obtained for Imp-450 sample compared to Imp-Dry and Imp-550 samples follow the same explanation. It is worth noting that the higher  $S_{\text{BJH}}$  values compared to  $S_{\text{BET}}$  values could be due to an under-estimation of the pore size via the BJH method (see Table 3). In this method, the considered size is the size for which the pore

empties (*i.e.* the aperture size of the pore), which does not correspond to the mean size of the pore in the case of bottle-like shape. Nevertheless, the relative magnitudes are consistent across the various results.

For the *in situ* method, the sample with and without proteins have been analyzed to study the potential templating effect of the protein. In both cases, a mixture of Types I and IV isotherms is observed. In contrast to the impregnation method, the smaller size of the hysteresis and the presence of a plateau prior to saturation suggest a much lower proportion of mesopores compared to micropores [49,50]. This is confirmed by the BJH distribution with a large proportion of micropores and a bimodal distribution of small mesopores (*i.e.* around 2.8 and 3.5 nm). In the case of the sample without proteins, no other pore size seems present. The microporous volume,  $V_{DR}$ , also present a similar value to the specific liquid volume adsorbed at the saturation pressure of nitrogen,  $V_p$  (representative only for microporous solids) (Table 3). On the opposite, in the case of the sample containing the protein, the hysteresis is larger and closes at higher relative pressure, which indicates the presence of a larger proportion of larger mesopores. The BJH distribution confirms this observation by the presence of supplementary size distributions (*i.e.* around 9.3 and 24.8 nm, and above 30 nm). These results are in opposition to those obtained by Reiner *et al.* (*i.e.* pores smaller than 5 nm, no BET isotherm) [30]. However, due to the small proportion of mesopores, it is probable that they were neglected by the authors.  $S_{BJH}$  and  $V_{BJH}$  values indicated in Table 3 for the IS samples are overestimated and not representative of the sample because the BJH method should be applied for a perfectly mesoporous solid while the IS sample is mainly microporous (Figure 2 (a-c)).

The mercury porosimetry curves (Figure 2(d)) highlight two successive behaviors for samples synthesized by the impregnation method. First, samples collapse under the mercury isostatic pressure at low pressure. Then, above a pressure of transition ( $P_t$ ), which is observed in the

mercury porosimetry curves by a change of slope, the mercury enters into the pores of the samples. Two models are used to describe these two phenomena and calculate the pore size distribution from mercury porosimetry measurements. Below  $P_t$ , Pirard's model is used to describe the collapse of larger pores [51]. Above  $P_t$ , Washburn's equation is applied for the mercury intrusion [50].

The cumulative volume distribution for pore sizes larger than 4 nm (*i.e.* STI size) is obtained by combining the nitrogen adsorption–desorption isotherms and the mercury porosimetry measurements. The total volume of the pores smaller than 2 nm is calculated by the Dubinin–Raduskevitch's method for micropores ( $V_{DR}$ , gas adsorption) and the BJH method for mesopores between 2 and 4 nm ( $V_{2-4nm}$ , gas adsorption). The pore size distribution is then determined using Pirard's and Washburn's models for pores larger than 4 nm ( $V_{Hg}$ , mercury porosimetry). The pore size distributions of the samples are displayed in Figure 2(e). The addition of the microporous volume ( $V_{DR}$ ), the cumulative volume of the pores between 2 and 4 nm ( $V_{2-4nm}$ ), and the specific pore volume obtained by mercury porosimetry ( $V_{Hg}$ ) gives the total cumulative volume ( $V_T$ ), summarized in Table 3.

The samples produced via the impregnation method are characterized by a broad size distribution with the presence of micropores, mesopores, and macropores. The distribution shifts towards the smaller pores when decreasing the amount of organic component in the sample (Imp-Dry > Imp-450 > Imp-550). This is probably due to the sintering process, as mentioned previously. On the other hand, the IS sample without protein mainly contains micropores and small mesopores (*i.e.*  $\leq 4$  nm). Indeed, 90 % of the pores are smaller than 8.5 nm. The total cumulative volume of pores,  $V_T$ , is also much smaller compared to the other samples (Table 3). Nevertheless, as indicated by the nitrogen adsorption-desorption analysis, the proportion of larger mesopores is higher in the

sample containing the protein. As shown in Figure 2(c), their size are larger than the protein size (4.5 x 4.5 x 4 nm, Table 1), allowing the diffusion of proteins outside of the pores.

For both encapsulation methods,  $V_p$  measured by nitrogen adsorption-desorption is greater than  $V_{Hg}$  determined by mercury porosimetry. This is linked to the presence of pores whose width is less than the limit size taken into account by the mercury porosimetry.

### 3.3. Determination of the Point of Zero Charge (PZC)

The evolutions of the final  $pH$  as a function of the initial  $pH$  curves (Figure 3) clearly show a plateau for all samples, which corresponds to the Point of Zero Charge (PZC) value (*i.e.* 9.5, 5.6, 5.4, and 6.5 respectively for Imp-Dry, Imp-450, Imp-550, and IS samples). The characterization of the PZC value allows the determination of the surface charge of the samples, which influences the “silica-protein” interactions and subsequently the protein release kinetics and the inhibitory activity. For silica samples, when  $pH < PZC$ , the surface charges of the sample are positive, characteristic of the presence of  $-OH_2^+$ ,  $-NH_2^+$ , and/or  $-NH_3^+$  surface groups. In contrast, when  $pH > PZC$ , the surface charges of the sample are negative, characteristic of the presence of  $-O^-$ ,  $-N^-$ , and/or  $-NH^-$  groups [52,53]. Following this reasoning, it is evident that the surface of Imp-Dry sample is positively charged at the  $pH$  of the release solution (*i.e.* 7.4, Figure 3) while Imp-450, Imp-550, and IS samples present a negative charge at their surface. The difference of PZC between Imp-Dry sample and the other samples is explained by the surface chemistry. On the one hand, ethylene diamine groups present at the surface of Imp-Dry sample are responsible for the high PZC value (*i.e.* 9.5) observed in Figure 3 ( $pK_a$  for the protonation of the amine groups into the corresponding ammonium form equal to 9.6) [62]. On the other hand, the presence of silanol groups and siloxane bridges at the surface of Imp-450, Imp-550, and IS samples explains the lower PZC value (between 5.4 and 6.5). Comparing to the literature, the PZC value measured for

Imp-Dry sample is similar to the PZC value found in the literature for silica gels containing amine groups (*i.e.* PZC around 10) [62]. On the opposite, the value measured for Imp-450, Imp-550, and IS samples is higher than the PZC value found in the literature for bare silica (*i.e.* PZC = 2-3) [69]. This indicates a larger proportion of siloxane groups (less acidic) compared to silanol groups (more acidic) [62]. For Imp-450 and Imp-550 samples, this larger proportion can be explained by the complete condensation of adjacent silanols at high temperature [61,62]. For IS sample, the presence of residual salt from the PBS leads to an increase in the PZC, which reaches 6.5.

### 3.4. Protein encapsulation

While no significant change is observed in the amount of encapsulated proteins for Imp-450 and Imp-550 samples between 3 h and 72 h of impregnation (Table 4), a significant increase (*i.e.* 30 %) is noticed for Imp-Dry sample. This difference in diffusion/adsorption kinetics of the protein can be attributed to the presence of the ethylene diamine groups that delays the diffusion of the proteins inside the pores via a steric hindrance effect and electrostatic interaction (*i.e.* positively charged surface and negatively charged protein). The difference in the quantity of protein adsorbed per unit mass between the samples seems rather explained by the difference in the specific surface area between the samples (Table 3) than by a difference in protein-silica affinity. Indeed, when calculating the quantity of protein adsorbed after 72 h per unit of specific surface area of silica, it is observed that the values for Imp-Dry and Imp-550 samples are close, while the quantity of protein per unit surface area of silica is smaller for Imp-450 sample (Table 4). This indicates that some proportion of surface area of the Imp-450 sample is not used for the protein adsorption. Nevertheless, these values are higher than the ones corresponding to the

adsorption of BMP-2 or STI at the surface of silica recorded in the literature (*i.e.* 0.5-4 mg<sub>protein</sub>/g<sub>Silica</sub>) [7,30,45].

In the case of the *in situ* method, it is assumed that the entire quantity of STI has been encapsulated inside or at the surface of the silica. The amount of encapsulated proteins is thus estimated from the amount of silica produced and the amount of STI added during the synthesis. The calculations show that the quantity of protein encapsulated via the *in situ* method (*i.e.* IS sample) is 5 to 9 times smaller than via the impregnation method. This quantity is directly fixed by the quantity of STI in the solution added during the gel synthesis and can therefore be controlled by regulating the concentration of the STI solution.

It is important to notice that these results represent the total amount of protein present inside and at the external surface of the samples and that they should be further contrasted in section 3.4. Nevertheless, the conclusions drawn regarding the relative magnitudes of encapsulation remains valid despite this remark.

### 3.5. Release test

#### 3.5.1. Release kinetics profiles

As previously mentioned, surface chemistry should be considered to adjust the release kinetics and protect the protein from denaturation. Surface chemistry of the pores can be tuned in order to incorporate specific functional groups [36–38]. These groups can specifically interact with the protein through electrostatic forces, hydrogen bonding, and van der Waals forces [35–38]. In principle, the local chemical environment can be tailored to promote the adsorption of the proteins while slowing down their diffusion inside the pores, without significantly altering their activity. The tuning of surface chemistry must be specifically adapted to the protein of interest,

*i.e.* in order to match its specific features, including surface charge distribution, size, secondary and tertiary structures, hydrophobicity, surface reactivity, etc..

Figures 4(a-c) illustrate the release kinetic profiles. In a clarity purpose, the results are divided in three parts: (a) profiles over 80 days, (b) zoom on the first 24 h of release, and (c) amount of STI released after the first day. This last subfigure is expressed as the percentage of STI remaining in the silica at day 1.

The release kinetics profiles (Figure 4(b)) highlight a fast release of STI from impregnation samples within the first 24 h. During this period, 40 % of the encapsulated STI are released. Due to the rapidity of this release, it is assumed that this burst is mostly affected by the fraction of the protein molecules that have only adsorbed on the external surface of the silica particles and not those that have penetrated inside the pores of silica. After immersion in the release medium, these biomolecules can easily and rapidly desorb from the silica particles. A remark must therefore be expressed regarding the results presented in Table 4. These results represent the total amount of protein present inside and at the external surface of the samples. Taking into account the results of this section, it seems that the proteins present at the surface of the silica accounts for about 40 % of the total amount. This means that the quantity of encapsulated proteins would vary between 8.5 and 13.9 mg<sub>STI</sub>/g<sub>Silica</sub>. Yet, the remarks expressed above regarding the relative magnitudes of encapsulation remains valid. In the case of Imp-450 sample, this probably explains the presence of surface area unused for the adsorption of protein. Indeed, if a large amount of proteins adsorbs on the external surface of silica particles, increasing the internal porosity will only lead to a small increase in the amount of adsorbed protein, resulting in the detection of a smaller amount of protein per unit of surface area (Table 4). Following the rational that the burst is probably due to STI adsorb at the surface, it was decided to express the rest of the profile as the proportion of the remaining STI in the silica at day 1 that is released in the medium (Figure 4(c)). Beyond day 1, a

sustained release of STI is observed to achieve a plateau at day 30 for the calcined samples at 450°C (Imp-450), *i.e.* release < 1% between day 30 and day 85 (Figures 4(a) and (c)). Regarding the sample calcined at 550°C (Imp-550), the release is also limited after day 30 but slightly higher than for Imp-450, *i.e.* release of 6 % between day 30 and day 85. This limitation in STI release, *i.e.* corresponding to 29 and 39 % of the amount of STI remaining at day 1 for Imp-450 and Imp-550 samples respectively, is not observed for Imp-Dry sample that still exhibits a sustained release beyond 80 days. This difference in release kinetics profile could be explained by the difference in surface chemistry of those samples. Indeed, while Imp-450 and Imp-550 samples bear negative charges, ethylene diamine groups of Imp-Dry sample provide positive charges at  $pH = 7.4$ . On the other hand, STI is negatively charged at this  $pH$ . Ethylene diamine groups present in Imp-Dry samples are thus able to interact with STI proteins via electrostatic interactions, preventing the proteins from rapidly diffusing from the pores towards the release solution. Tang *et al.* previously studied the encapsulation and release of BMP-2 in unmodified silica. They showed the presence of a large burst (*i.e.* 20-65 %) followed by a constant delivery over 28 days [45].

In contrast, the IS sample presents a small release over the first 24 h and a slower release until day 30, indicating that a large proportion of the proteins are encapsulated inside the particles (Figure 4(b)). The amount of proteins present at the surface of the silica can therefore be neglected and it can be considered that the results presented in Table 4 only accounts for the encapsulated proteins. After day 30, a plateau establishes at 37 % of the amount of STI remaining at day 1, *i.e.* release < 1% between day 30 and day 85 (Figures 4(a) and (c)). This plateau can be explained by a physical entrapment of STI inside closed pores. A previous study by Reiner *et al.* also highlighted this constant delivery over 30 days [30]. However, only qualitative comparison



can be performed with this study because of the differences in the release conditions (mainly the pH and the silica/release medium ratio).

It is important to notice that these results were obtained in *in vitro* conditions. Nevertheless, previous studies highlighted a fast *in vivo* degradation of silica nanoparticles in zebrafishes [70,71]. The reader must therefore keep in mind that these results could further influence the release kinetics.

### 3.5.2. Activity of released STI

The inhibitory activity of STI released after 30 min, 1 week, and 4 weeks is expressed in terms of ratio of active proteins to the total amount of proteins released (Figure 4(d)). In view of the previous results presented in Section 3.5.1, Imp-Dry, Imp-550, and IS samples were chosen. For IS sample, only results after 1 week of release could be measured due to the low concentration of protein released in solution compared to the sensitivity of the bioassay.

For Imp-Dry and Imp-550 samples, a significant difference is noticed in the percentage of active released protein between the first sampling period at 30 min and 1 week later (Figure 4(d)). While the fraction of enzyme released after 30 min is mostly active, after 1 week of incubation, the specific activity of STI released decreases below 40 %. This loss in protein activity is only explained by a change in its conformation. Accordingly, we could anticipate that when more deeply internalized within the pore size of silica, the protein could partially unfold through its interactions with the pore walls. This denaturation is still more accentuated after 4 weeks of incubation where STI released from Imp-550 sample does not give any inhibitory signal. In contrast, the specific activity of STI released from Imp-Dry remains close to the value observed after 1 week of incubation (*i.e.* 30 %). This difference in evolution in protein stability between

these two samples could be explained by the difference in surface chemistry. In the case of Imp-550 sample, the silanol groups present at the surface of the walls interact with STI via electrostatic interactions, causing change in the protein conformation [72]. In Imp-Dry sample, ethylene diamine groups protect the proteins from these interactions, leading to a conservation of some activity.

For IS sample, the protein appears to retain its activity after 1 week of release. This is probably due to the presence of pores with size comparable to the protein size. In this case, the pore walls could physically restrict protein motions and prevent the unfolding of the protein [73].

In addition to the release, the studies mentioned in the Section 3.5.1., also focus on the protein activity. On the one hand, Tang *et al.* have highlighted a small change in protein conformation (*i.e.* 3.5 %). On the other hand, the results of Reiner *et al.* have indicated that STI is greatly affected by the *pH* of the release medium. Song *et al.* have notably found that *pH* can affect the conformation of the reactive loop of STI by disturbing the hydrogen bonds of this loop [74]. As shown in Section 3.3., the silica samples can influence the *pH* of the release medium. Moreover, the storage of the samples might also have an impact as Thorat *et al.* have showed that the frozen treatment of PBS can decrease the *pH* solution in frozen state by over 4 *pH* units [75].

#### 4. CONCLUSIONS

In conclusion, silica gels were synthesized via two methods (*i.e.* an impregnation method and an *in situ* method) for the encapsulation and release of STI. Through control of the drying/calcination conditions, the impregnation method allowed the preparation of three types of silica gels: Imp-Dry, Imp-450, and Imp-550. This method allows more freedom for the design of

the silica matrix because the protein is added after the synthesis and thermal treatments of silica matrix. A fine tuning of the textural morphology and surface chemistry is achieved by modulating the synthesis conditions such as *pH*, solvent, temperature, hydrolysis ratio, dilution ratio, and the use of functionalized molecules EDAS. However, this technique is more time consuming because the adsorption of STI protein is realized in a second time.

In contrast, the *in situ* method involves a one-pot synthesis allowing the direct incorporation of the protein during the silica gel synthesis, reducing the processing time [35]. However, due to their high molecular weight, proteins can be firmly trapped inside the matrix network. Moreover, due to the presence of the protein in the sol, the conventional synthesis parameters (*i.e.* extreme *pH*, high temperature, and non-aqueous solvent) must be adapted to prevent any denaturation of the protein. These conditions therefore limit the optimization of the silica matrix.

In this study, it is shown that the synthesis method of silica samples significantly influences the surface chemistry, charge density, and textural properties of silica samples. Indeed, while a large range of pore sizes were measured for silica gels prepared by impregnation (*i.e.* micro-, meso- and macropores), the IS silica sample was mainly composed of micropores. Furthermore, for the impregnation method, the thermal treatments (*i.e.* only drying or drying+calcination) of silica samples also influence the surface chemistry, charge density, and PZC value. Indeed, for only dried silica sample, the PZC is equal to 9.5 due to the presence of amino groups from EDAS molecules. When silica samples are dried and calcined, the PZC value decreases to 5.5, with the degradation of amino groups and the increase of silanols and siloxanes bond contents. All these differences in porosity and surface chemistry of silica have been shown to significantly affect the immobilization efficiency of STI, its release kinetics profile, but also the protection of its conformation and inhibitory activity. Although limited to a number of experimental criteria, this

study has demonstrated the opportunity to control the sustained release of STI over a period of at least 40 days according to release kinetics profiles, which can be adjusted as a function of textural properties and the surface nature of the silica samples.

It is worthwhile to notice that the two encapsulation techniques used can be easily extend to other proteins. The reader must nevertheless keep in mind that protein-substrates interactions are linked to the nature of the protein and more specifically to its size, hydrophobicity, charge etc. Changing the protein might therefore lead to different results than those presented here.

## 5. ACKNOWLEDGMENTS

Funding: This work was supported by the Fund for Scientific Research (FNRS) under a Fund for Research Training in Industry and Agriculture (FRIA) grant.

Stéphanie D. Lambert thanks the F.R.S.-FNRS for her Senior Research Associate position.

## 6. CONFLICT OF INTEREST

The authors declare that there is no conflict of interest concerning this work.

## 7. REFERENCES

- [1] R. Dimitriou, E. Jones, D. McGonagle, P. V. Giannoudis, Bone regeneration: current concepts and future directions, *BMC Med.* 9 (2011) 66. doi:10.1186/1741-7015-9-66.
- [2] W. Wang, K.W.K. Yeung, Bone grafts and biomaterials substitutes for bone defect repair: A review, *Bioact. Mater.* 2 (2017) 224–247. doi:10.1016/j.bioactmat.2017.05.007.

- [3] J.E. Schroeder, R. Mosheiff, Tissue engineering approaches for bone repair: Concepts and evidence, *Injury*. 42 (2011) 609–613. doi:10.1016/j.injury.2011.03.029.
- [4] A.S. Brydone, D. Meek, S. MacLaine, Bone grafting, orthopaedic biomaterials, and the clinical need for bone engineering, *Proc. Inst. Mech. Eng. Part H J. Eng. Med.* 224 (2010) 1329–1343. doi:10.1243/09544119JEIM770.
- [5] V. Campana, G. Milano, E. Pagano, M. Barba, C. Cicione, G. Salonna, W. Lattanzi, G. Logroscino, Bone substitutes in orthopaedic surgery: from basic science to clinical practice, *J. Mater. Sci. Mater. Med.* 25 (2014) 2445–2461. doi:10.1007/s10856-014-5240-2.
- [6] US Census Bureau, Statistical abstracts of the United States: 2012 - Section 1. Population, (2012).  
[www.census.gov/library/publications/2011/compendia/statab/131ed/population.html](http://www.census.gov/library/publications/2011/compendia/statab/131ed/population.html)  
(accessed November 25, 2019).
- [7] E.M. Santos, S. Radin, P. Ducheyne, Sol-gel derived carrier for the controlled release of proteins, *Biomaterials*. 20 (1999) 1695–1700. doi:10.1016/S0142-9612(99)00066-6.
- [8] R.G. Tilkin, J.G. Mahy, N. Régibeau, C. Grandfils, S.D. Lambert, Optimization of Synthesis Parameters for the Production of Biphasic Calcium Phosphate Ceramics via Wet Precipitation and Sol-Gel Process, *ChemistrySelect*. 4 (2019) 6634–6641.  
doi:10.1002/slct.201901175.
- [9] T.D. Roy, J.L. Simon, J.L. Ricci, E.D. Rekow, V.P. Thompson, J.R. Parsons, Performance of degradable composite bone repair products made via three-dimensional fabrication techniques, *J. Biomed. Mater. Res. Part A*. 66A (2003) 283–291. doi:10.1002/jbm.a.10582.

- [10] X. Li, X. Liu, S. Wu, K.W.K. Yeung, Y. Zheng, P.K. Chu, Design of magnesium alloys with controllable degradation for biomedical implants : From bulk to surface, *Acta Biomater.* 45 (2016) 2–30. doi:10.1016/j.actbio.2016.09.005.
- [11] S. Bhattacharyya, H. Wang, P. Ducheyne, Polymer-coated mesoporous silica nanoparticles for the controlled release of macromolecules, *Acta Biomater.* 8 (2012) 3429–3435. doi:10.1016/j.actbio.2012.06.003.
- [12] S. Chen, X. Shi, H. Morita, J. Li, N. Ogawa, T. Ikoma, S. Hayakawa, Y. Shirosaki, A. Osaka, N. Hanagata, BMP-2-loaded silica nanotube fibrous meshes for bone generation, *Sci. Technol. Adv. Mater.* 12 (2011) 065003. doi:10.1088/1468-6996/12/6/065003.
- [13] K.W. Lo, B.D. Ulery, K.M. Ashe, C.T. Laurencin, Studies of bone morphogenetic protein-based surgical repair, *Adv. Drug Deliv. Rev.* 64 (2012) 1277–1291. doi:10.1016/j.addr.2012.03.014.
- [14] C.J. Hwang, A.R. Vaccaro, J.P. Lawrence, J. Hong, H. Schellekens, M.H. Alaoui-Ismaili, D. Falb, Immunogenicity of bone morphogenetic proteins, *J. Neurosurg. Spine SPI.* 10 (2009) 443–551. doi:10.3171/2009.1.SPINE08473.
- [15] P.C. Bessa, M. Casal, R.L. Reis, Bone morphogenetic proteins in tissue engineering: the road from laboratory to clinic , part II (BMP delivery), *J. Tissue Eng. Regen. Med.* 2 (2008) 81–96. doi:10.1002/term.
- [16] Y. Kimura, D. Ph, N. Miyazaki, M. Eng, N. Hayashi, M. Eng, Controlled Release of Bone Morphogenetic Protein-2 Enhances Recruitment of Osteogenic Progenitor Cells for De Novo Generation of Bone Tissue, *Tissue Eng. Part A.* 16 (2010) 1263–1270. doi:10.1089/ten.tea.2009.0322.

- [17] J. Yamashita, B.R. Furman, H.R. Rawls, X. Wang, C.M. Agrawal, The use of dynamic mechanical analysis to assess the viscoelastic properties of human cortical bone., J. Biomed. Mater. Res. 58 (2001) 47–53. doi:10.1002/1097-4636(2001)58:1<47::AID-JBM70>3.0.CO;2-U.
- [18] J. Sun, J. Li, C. Li, Y. Yu, Role of bone morphogenetic protein-2 in osteogenic differentiation of mesenchymal stem cells, Mol. Med. Rep. 12 (2015) 4230–4237. doi:10.3892/mmr.2015.3954.
- [19] Y. Zhang, Y. Ma, M. Yang, S. Min, J. Yao, L. Zhu, Expression , purification , and refolding of a recombinant human bone morphogenetic protein 2 in vitro, Protein Expr. Purif. 75 (2011) 155–160. doi:10.1016/j.pep.2010.07.014.
- [20] H. Jung, S. Yook, C. Han, T. Jang, H. Kim, Y. Koh, Y. Estrin, Highly aligned porous Ti scaffold coated with bone morphogenetic protein-loaded silica / chitosan hybrid for enhanced bone regeneration, J. Biomed. Mater. Res. Part B Appl. Biomater. 102B (2014) 913–921. doi:10.1002/jbm.b.33072.
- [21] J.A. Schrier, P.P. Deluca, Recombinant Human Bone Morphogenetic Protein-2 Binding and Incorporation in PLGA Microsphere Delivery Systems, Pharm. Dev. Technol. 4 (1999) 611–621. doi:10.1081/PDT-100101400.
- [22] M.R. Johnson, H. Lee, R. V Bellamkonda, R.E. Guldberg, Sustained release of BMP-2 in a lipid-based microtube vehicle, Acta Biomater. 5 (2009) 23–28. doi:10.1016/j.actbio.2008.09.001.
- [23] Y. Li, Y. Song, A. Ma, C. Li, Surface Immobilization of TiO<sub>2</sub> Nanotubes with Bone Morphogenetic Protein-2 Synergistically Enhances Initial Preosteoblast Adhesion and

- Osseointegration, *Biomed Res. Int.* 2019 (2019) 5697250. doi:10.1155/2019/5697250.
- [24] M.I. Vlasenkova, E.S. Dolinina, E. V Parfenyuk, Preparation of mesoporous silica microparticles by sol-gel/emulsion route for protein release, *Pharm. Dev. Technol.* 24 (2018) 243–252. doi:10.1080/10837450.2018.1457051.
- [25] W. Yang, B. Hellner, F. Baneyx, Self-Immobilization of Car9 Fusion Proteins within High Surface Area Silica Sol-Gels and Dynamic Control of Protein Release, *Bioconj. Chem.* 27 (2016) 2450–2459. doi:10.1021/acs.bioconjchem.6b00406.
- [26] G. Tonon, M. Morpurgo, Sol-gel derived silica polymers for the sustained release of proteins, EP2004727, 2008.
- [27] Y.C. Chen, T. Smith, R.H. Hicks, A. Doekhie, F. Koumanov, S.A. Wells, K.J. Edler, J. Van Den Elsen, G.D. Holman, K.J. Marchbank, A. Sartbaeva, Thermal stability, storage and release of proteins with tailored fit in silica, *Sci. Rep.* 7 (2017) 1–8. doi:10.1038/srep46568.
- [28] Y.-C. Chen, C.-P. Liu, C.-K. Yang, B.-Y. Huang, C.-Y. Liu, Preparation and Release Properties of Sol-Gel Encapsulated Proteins, *J. Anal. Sci. Methods Instrum.* 03 (2013) 11–16. doi:10.4236/jasmi.2013.33A002.
- [29] J. Zdarta, K. Sałek, A. Kołodziejczak-radzimska, K. Siwińska-stefańska, K. Szwarc-rzepka, M. Norman, Ł. Kłapiszewski, P. Bartczak, E. Kaczorek, T. Jesionowski, Immobilization of Amano Lipase A onto Stöber silica surface: process characterization and kinetic studies, *Open Chem.* 13 (2015) 138–148. doi:10.1515/chem-2015-0017.
- [30] T. Reiner, S. Kababya, I. Gotman, Protein incorporation within Ti scaffold for bone ingrowth using Sol-gel SiO<sub>2</sub> as a slow release carrier, *J. Mater. Sci. Mater. Med.* 19 (2008)



- 583–589. doi:10.1007/s10856-007-3194-3.
- [31] L. Ronda, S. Bruno, B. Campanini, A. Mozzarelli, S. Abbruzzetti, Immobilization of Proteins in Silica Gel: Biochemical and Biophysical Properties, *Curr. Org. Chem.* 19 (2015) 15–18. doi:10.2174/1385272819666150601211349.
- [32] C.J. Brinker, G.W. Scherer, *Sol-Gel Science: The Physics and Chemistry of Sol-Gel Processing*, Academic Press, San Diego, CA, 1990. doi:10.1016/B978-0-08-057103-4.50006-4.
- [33] S. Lambert, C. Alié, J.P. Pirard, B. Heinrichs, Study of textural properties and nucleation phenomenon in Pd/SiO<sub>2</sub>, Ag/SiO<sub>2</sub> and Cu/SiO<sub>2</sub> cogelled xerogel catalysts, *J. Non. Cryst. Solids.* 342 (2004) 70–81. doi:10.1016/j.jnoncrysol.2004.06.005.
- [34] T. Andreani, A.L.R. de Souza, A.M. Silva, E.B. Souto, Sol–Gel Carrier System: A Novel Controlled Drug Delivery, in: E.B. Souto (Ed.), *Patenting Nanomedicines Leg. Asp. Intellect. Prop. Grant Oppor.*, Springer-Verlag Berlin Heidelberg, Heidelberg, 2012: pp. 1551–1660. doi:10.1007/978-3-642-29265-1.
- [35] X. Wang, N. Ben Ahmed, G.S. Alvarez, M. V Tuttolomondo, C. Hélyary, M.F. Desimone, T. Coradin, Sol-Gel Encapsulation of Biomolecules and Cells for Medicinal Applications, *Curr. Top. Med. Chem.* 15 (2015) 223–244. doi:10.2174/1568026614666141229112734.
- [36] W. Jin, J.D. Brennan, Properties and applications of proteins encapsulated within sol-gel derived materials, *Anal. Chim. Acta.* 461 (2002) 1–36. doi:10.1016/S0003-2670(02)00229-5.
- [37] A.M. Anderson, M.K. Carroll, E.C. Green, J.T. Melville, M.S. Bono, Hydrophobic silica aerogels prepared via rapid supercritical extraction, *J. Sol-Gel Sci. Technol.* 53 (2010)

- 199–207. doi:10.1007/s10971-009-2078-z.
- [38] Z. Shao, X. Cheng, Y. Zheng, Facile co-precursor sol-gel synthesis of a novel amine-modified silica aerogel for high efficiency carbon dioxide capture, *J. Colloid Interface Sci.* 530 (2018) 412–423. doi:10.1016/j.jcis.2018.06.094.
- [39] Q. He, J. Shi, M. Zhu, Y. Chen, F. Chen, The three-stage in vitro degradation behavior of mesoporous silica in simulated body fluid, *Microporous Mesoporous Mater.* 131 (2010) 314–320. doi:10.1016/j.micromeso.2010.01.009.
- [40] J. Livage, T. Coradin, C. Roux, Encapsulation of biomolecules in silica gels, *J. Phys. Condens. Matter.* 13 (2001) R673–R691. doi:10.1088/0953-8984/13/33/202.
- [41] J. Hum, A.R. Boccaccini, Bioactive glasses as carriers for bioactive molecules and therapeutic drugs : a review, *J. Mater. Sci. Mater. Med.* 23 (2012) 2317–2333. doi:10.1007/s10856-012-4580-z.
- [42] C.M. Agrawal, J. Best, J.D. Heckman, B.D. Boyan, Protein release kinetics of a biodegradable implant for fracture, *Biomaterials.* 16 (1995) 1255–1260. doi:10.1016/0142-9612(95)98133-Y.
- [43] A. Chaudhari, C. Mv, J. Martens, K. Vandamme, I. Naert, D.J. Bone, Bone tissue response to BMP-2 adsorbed on amorphous microporous silica implants, *J. Clin. Periodontol.* 39 (2012) 1206–1213. doi:10.1111/jcpe.12005.
- [44] A. Chaudhari, J. Duyck, A. Braem, J. Vleugels, H.P.D. Logeart-avramoglou, I. Naert, J.A. Martens, K. Vandamme, Modified Titanium Surface-Mediated Effects on Human Bone Marrow Stromal Cell Response, *Materials (Basel).* 2 (2013) 5533–5548. doi:10.3390/ma6125533.

- [45] W. Tang, D. Lin, Y. Yu, H. Niu, H. Guo, Y. Yuan, C. Liu, Bioinspired trimodal macro / micro / nano-porous scaffolds loading rhBMP-2 for complete regeneration of critical size bone defect, *Acta Biomater.* 32 (2016) 309–323. doi:10.1016/j.actbio.2015.12.006.
- [46] X. Li, W. Lin, F. Xing, The Degradation and BMP release Dynamics of Silica-based Xerogels Modified by adding Calcium and Magnesium or Sintering Process, *Appl. Mech. Mater.* 151 (2012) 378–382. doi:10.4028/www.scientific.net/AMM.151.378.
- [47] S.B. Nicoll, S. Radin, E.M. Santos, R.S. Tuan, P. Ducheyne, In vitro release kinetics of biologically active transforming growth factor- $\beta$ 1 from a novel porous glass carrier, *Biomaterials.* 18 (1997) 853–859. doi:10.1016/S0142-9612(97)00008-2.
- [48] J.G. Mahy, L. Tasseroul, A. Zubiaur, J. Geens, M. Brisbois, M. Herlitschke, R. Hermann, B. Heinrichs, S.D. Lambert, Highly dispersed iron xerogel catalysts for p-nitrophenol degradation by photo-Fenton effects, *Microporous Mesoporous Mater.* 197 (2014) 164–173. doi:10.1016/j.micromeso.2014.06.009.
- [49] A. Lecloux, Exploitation des isothermes d'adsorption et de désorption d'azote pour l'étude de la texture des solides poreux, *Mémoires Société Des Sci. Liege.* 4 (1971) 169–209.
- [50] A. Lecloux, Texture of Catalysts, in: J.R. Anderson, M. Boudart (Eds.), *Catal. Sci. Technol.* Vol. 2, Springer, Berlin, 1981: p. 171. doi:10.1007/978-3-642-93247-2.
- [51] R. Pirard, B. Heinrichs, O.V.A.N. Cantfort, J.P. Pirard, Mercury Porosimetry Applied to Low Density Xerogels ; Relation between Structure and Mechanical Properties, *J. Sol-Gel Sci. Technol.* 13 (1998) 335–339. doi:10.1023/A:1008676211157.
- [52] J. Park, J.R. Regalbuto, A Simple, Accurate Determination of Oxide PZC and the Strong Buffering Effect of Oxide Surfaces at Incipient Wetness, *J. Colloid Interface Sci.* 175

- (1995) 239–252. doi:10.1006/jcis.1995.1452.
- [53] S. Lambert, N. Job, L.D. Souza, M. Fernando, R. Pereira, R. Pirard, B. Heinrichs, J. Luis, J. Pirard, J.R. Regalbuto, Synthesis of very highly dispersed platinum catalysts supported on carbon xerogels by the strong electrostatic adsorption method, *J. Catal.* 261 (2009) 23–33. doi:10.1016/j.jcat.2008.10.014.
- [54] O.H. Lowry, N.J. Rosebrough, L.A. Farr, R.J. Randall, Protein measurement with the folin phenol reagent, *J. Biol. Chem.* 193 (1951) 265–275. doi:10.1016/0304-3894(92)87011-4.
- [55] Merck, Enzymatic Assay of Trypsin Inhibitor, (2020).  
<https://www.sigmaaldrich.com/technical-documents/protocols/biology/enzymatic-assay-of-trypsin-inhibitor.html> (accessed April 27, 2018).
- [56] H. Mansur, R. Oréfice, M. Pereira, Z. Lobato, FTIR and UV-vis study of chemically engineered biomaterial surfaces for protein immobilization, *Spectroscopy*. 16 (2002) 351–360. doi:10.1155/2002/183053.
- [57] E. Péré, H. Cardy, O. Cairon, M. Simon, S. Lacombe, Quantitative assessment of organic compounds adsorbed on silica gel by FTIR and UV-VIS spectroscopies: the contribution of diffuse reflectance spectroscopy, *Vib. Spectrosc.* 25 (2001) 163–175.  
doi:10.1016/S0924-2031(00)00113-2.
- [58] R. Antony, S. Theodore David Manickam, P. Kollu, P.V. Chandrasekar, K. Karruppasamy, S. Balakumar, Highly dispersed Cu(II), Co(II) and Ni(II) catalysts covalently immobilized on imine-modified silica for cyclohexane oxidation with hydrogen peroxide, *RSC Adv.* 4 (2014) 24820–24830. doi:10.1039/C4RA01960A.
- [59] L.B. Capeletti, I.M. Baibich, I.S. Butler, J.H.Z. dos Santos, Infrared and Raman

- spectroscopic characterization of some organic substituted hybrid silicas, *Spectrochim. Acta Part A Mol. Biomol. Spectrosc.* 133 (2014) 619–625. doi:10.1016/j.saa.2014.05.072.
- [60] J. Osswald, K.T. Fehr, FTIR spectroscopic study on liquid silica solutions and nanoscale particle size determination, *J. Mater. Sci.* 41 (2006) 1335–1339. doi:10.1007/s10853-006-7327-8.
- [61] S.L. Warring, D.A. Beattie, A.J. Mcquillan, Surface Siloxane-to-Silanol Interconversion during Room-Temperature Hydration/Dehydration of Amorphous Silica Films Observed by ATR-IR and TIR-Raman Spectroscopy, *Langmuir*. 32 (2016) 1568–1576. doi:10.1021/acs.langmuir.5b04506.
- [62] M. Etienne, A. Walcarius, Analytical investigation of the chemical reactivity and stability of aminopropyl-grafted silica in aqueous medium, *Talanta*. 59 (2003) 1173–1188. doi:10.1016/S0039-9140(03)00024-9.
- [63] L. Adumeau, C. Genevois, L. Roudier, C. Schatz, L. Adumeau, C. Genevois, L. Roudier, C. Schatz, F. Couillaud, Impact of surface grafting density of PEG macromolecules on dually fluorescent silica nanoparticles used for the in vivo imaging of subcutaneous tumors, *Biochim. Biophys. Acta*. 1861 (2017) 1587–1596. doi:10.1016/j.bbagen.2017.01.036.
- [64] S. Bharathi, N. Fishelson, O. Lev, Direct Synthesis and Characterization of Gold and Other Noble Metal Nanodispersions in Sol - Gel-Derived Organically Modified Silicates, *Langmuir*. 15 (1999) 1929–1937. doi:10.1021/la980490x.
- [65] L.T. Zhuravlev, Concentration of Hydroxyl Groups on the Surface of Amorphous Silicas, *Langmuir*. 3 (1987) 316–318. doi:10.1021/la00075a004.

- [66] D.J. Belton, O. Deschaume, C.C. Perry, An overview of the fundamentals of the chemistry of silica with relevance to biosilicification and technological advances, *FEBS J.* 279 (2012) 1710–1720. doi:10.1111/j.1742-4658.2012.08531.x.An.
- [67] M. Thommes, K. Kaneko, A. V Neimark, J.P. Olivier, F. Rodriguez-reinoso, J. Rouquerol, K.S.W. Sing, Physisorption of gases, with special reference to the evaluation of surface area and pore size distribution (IUPAC Technical Report), *Pure Appl. Chem.* 87 (2015) 1051–1069. doi:10.1515/pac-2014-1117.
- [68] C. Alié, F. Ferauche, R. Pirard, A.J. Lecloux, J.-P. Pirard, Preparation of low-density xerogels by incorporation of additives during synthesis, *J. Non. Cryst. Solids.* 289 (2001) 88–96. doi:10.1016/S0022-3093(01)00697-4.
- [69] M. Kosmulski, Compilation of PZC and IEP of sparingly soluble metal oxides and hydroxides from literature, *Adv. Colloid Interface Sci.* 152 (2009) 14–25. doi:10.1016/j.cis.2009.08.003.
- [70] D. Cassano, A.-K. Mapanao, M. Summa, Y. Vlamidis, G. Giannone, M. Santi, E. Guzzolino, L. Pitto, L. Polisenio, R. Bertorelli, V. Voliani, Biosafety and Biokinetics of Noble Metals: The Impact of Their Chemical Nature, *ACS Appl. Biomater.* 2 (2019) 4464–4470. doi:10.1021/acsabm.9b00630.
- [71] D. Cassano, D.R. Martir, G. Signore, V. Piazzaa, V. Voliani, Biodegradable hollow silica nanospheres containing gold nanoparticle arrays, *Chem. Commun.* 51 (2015) 9939–9942. doi:10.1039/C5CC02771C.
- [72] A. Yildirim, E. Ozgur, M. Bayindir, Impact of mesoporous silica nanoparticle surface functionality on hemolytic activity, thrombogenicity and non-specific protein adsorption,

- J. Mater. Chem. B. 1 (2013) 1909–1920. doi:10.1039/c3tb20139b.
- [73] D.M. Schlipf, S.E. Rankin, B.L. Knutson, Pore-Size Dependent Protein Adsorption and Protection from Proteolytic Hydrolysis in Tailored Mesoporous Silica Particles, ACS Appl. Mater. Interfaces. 5 (2013) 10111–10117. doi:10.1021/am402754h.
- [74] H.K. Song, S.W. Suh, Kunitz-type Soybean Trypsin Inhibitor Revisited : Refined Structure of its Complex with Porcine Trypsin Reveals an Insight into the Interaction Between a Homologous Inhibitor from *Erythrina caffra* and Tissue-type Plasminogen Activator, J. Mol. Biol. 275 (1998) 347–363. doi:10.1006/jmbi.1997.1469.
- [75] A.A. Thorat, R. Suryanarayanan, Characterization of Phosphate Buffered Saline (PBS) in Frozen State and after Freeze-Drying, Pharm. Res. 36 (2019) 98. doi:10.1007/s11095-019-2619-2.
- [76] C. Scheufler, W. Sebal, M. Hülsmeier, Crystal structure of human bone morphogenetic protein-2 at 2.7 Å resolution<sup>1</sup>, J. Mol. Biol. 287 (1999) 103–115. doi:10.1006/jmbi.1999.2590.
- [77] Y. Chang, T.C. Liu, M. Tsai, Selective Isolation of Trypsin Inhibitor and Lectin from Soybean Whey by Chitosan / Tripolyphosphate / Genipin Co-Crosslinked Beads, Int. J. Mol. Sci. 15 (2014) 9979–9990. doi:10.3390/ijms15069979.
- [78] J. Yang, P. Shi, M. Tu, Y. Wang, M. Liu, F. Fan, M. Du, Bone morphogenetic proteins: Relationship between molecular structure and their osteogenic activity, Food Sci. Hum. Wellness. 3 (2014) 127–135. doi:10.1016/j.fshw.2014.12.002.

## 8. TABLES

**Table 1.** Properties of STI and BMP-2

	<b>STI</b>	<b>BMP-2</b>
Molecular weight (g/mol)	21,000 [7,30]	26,000 [30]
Size (nm)	4.5 x 4.2 x 4 [74]	7 x 3.5 x 3 [76]
Point of zero charge ( <i>pH</i> unit)	4.5 [77]	4.8-5.1 [78]



**Table 2.** Weight decrease of the samples measured by TGA.

<b>Sample</b>	<b>Weight loss (wt%)</b>
Imp-Dry	21
Imp-450	4
Imp-550	3
IS-Blank	4

**Table 3.** Textural properties of silica gels.

Sample	$S_{\text{BET}}$ (m <sup>2</sup> /g) ± 5	$V_{\text{P}}$ (cm <sup>3</sup> /g) ± 0.1	$V_{\text{DR}}$ (cm <sup>3</sup> /g) ± 0.01	$V_{\text{BJH}}$ (cm <sup>3</sup> /g) ± 0.01	$S_{\text{BJH}}$ (cm <sup>2</sup> /g) ± 5	$V_{\text{Hg}}$ (cm <sup>3</sup> /g) ± 0.1	$P_{\text{t}}$ (MPa)	$k$ (nm MPa <sup>0.25</sup> )	$V_{2-4\text{nm}}$ (cm <sup>3</sup> /g) ± 0.001	$V_{\text{T}}$ (cm <sup>3</sup> /g) ± 0.1
Imp-Dry	330	1.5	0.19	1.47	440	1.3	26.3	129	0.026	1.5
Imp-450	585	1.7	0.26	1.67	535	1.2	44.7	87	0.032	1.5
Imp-550	445	1.5	0.22	1.47	475	1.3	56.3	73	0.034	1.6
IS	545	0.3	0.25	0.18*	265*	0.1	34.4	106	0.168	0.5
IS-Prot	590	0.4	0.28	0.24*	325*	/	/	/	/	/

Note:  $S_{\text{BET}}$ : specific surface area determined by the BET method;  $V_{\text{P}}$ : specific liquid volume adsorbed at the saturation pressure of nitrogen;  $V_{\text{DR}}$ : specific micropore volume determined by the Dubinin–Raduskevitch theory;  $V_{\text{BJH}}$ : specific mesoporous volume determined by the Barrett, Joyner, and Halenda theory;  $S_{\text{BJH}}$ : specific mesoporous surface determined by the Barrett, Joyner and Halenda theory;  $V_{\text{Hg}}$ : specific pore volume measured by mercury porosimetry;  $P_{\text{t}}$ : pressure of change of mechanism during mercury porosimetry (change from collapse to intrusion) ;  $k$ : buckling model constant;  $V_{2-4\text{nm}}$ : cumulative volume pores of diameter between 2 and 4 nm determined by the Barrett, Joyner, and Halenda theory;  $V_{\text{T}}$ : total pore volume obtained by addition of  $V_{\text{DR}}$ ,  $V_{2-4\text{nm}}$ , and  $V_{\text{Hg}}$ .

\* = not representative of the sample ; / = not measured.

**Table 4.** Amount of proteins encapsulated.

	3 hours of impregnation		72 h of impregnation (Imp) or encapsulation (IS)	
Sample	$m_{STI}/m_{Silica}$ (mg <sub>STI</sub> /g <sub>Silica</sub> )	$m_{STI}/S_{BET}$ (μg <sub>STI</sub> /m <sup>2</sup> )	$m_{STI}/m_{Silica}$ (mg <sub>STI</sub> /g <sub>Silica</sub> )	$m_{STI}/S_{BET}$ (μg <sub>STI</sub> /m <sup>2</sup> )
Imp-Dry	14.2 ± 0.7	42.4 ± 2.0	18.7 ± 0.1	55.9 ± 0.3
Imp-450	22.9 ± 0.3	38.9 ± 0.4	23.2 ± 0.9	39.4 ± 1.6
Imp-550	23.3 ± 0.1	51.2 ± 0.3	23.7 ± 1.1	52.1 ± 2.3
IS	/	/	3.8	6.3




Note: / = not relevant

## 9. FIGURE CAPTURES

**Figure 1.** FTIR spectra of silica gels: ✕ Imp-Dry, ▲ Imp-450, ◆ Imp-550, ■ IS-Blank. (a) Zone 400-1300  $\text{cm}^{-1}$ , (b) zone 1300-1700  $\text{cm}^{-1}$ , (c) zone 2600-3800  $\text{cm}^{-1}$ .

**Figure 2.** Porosity analysis: ✕ Imp-Dry, ▲ Imp-450, ◆ Imp-550, ■ IS-Blank, ● IS-Prot. (a) Nitrogen adsorption-desorption isotherms, (b-c) pore size distribution determined from the nitrogen adsorption-desorption isotherms, (d) mercury porosimetry curves, (e) pore size distributions determined from the nitrogen adsorption-desorption isotherms and the mercury porosimetry curves.

**Figure 3.** PZC determination of silica gels: ✕ Imp-Dry, ▲ Imp-450, ◆ Imp-550, ■ IS-Blank. The full line represents the pH of the release solution (*i.e.* pH = 7.4).

**Figure 4.** (a-c) Release kinetics profile of STI from silica gels: ✕ Imp-Dry, ▲ Imp-450, ◆ Imp-550, ■ IS. (a) Release kinetics profile (b) Zoom on the possible burst (0 to 1 day) (c) Profile of the STI released after the first day. (d) Remaining activity after  30 min,  1 week, and  4 weeks of release.

## 10. FIGURES

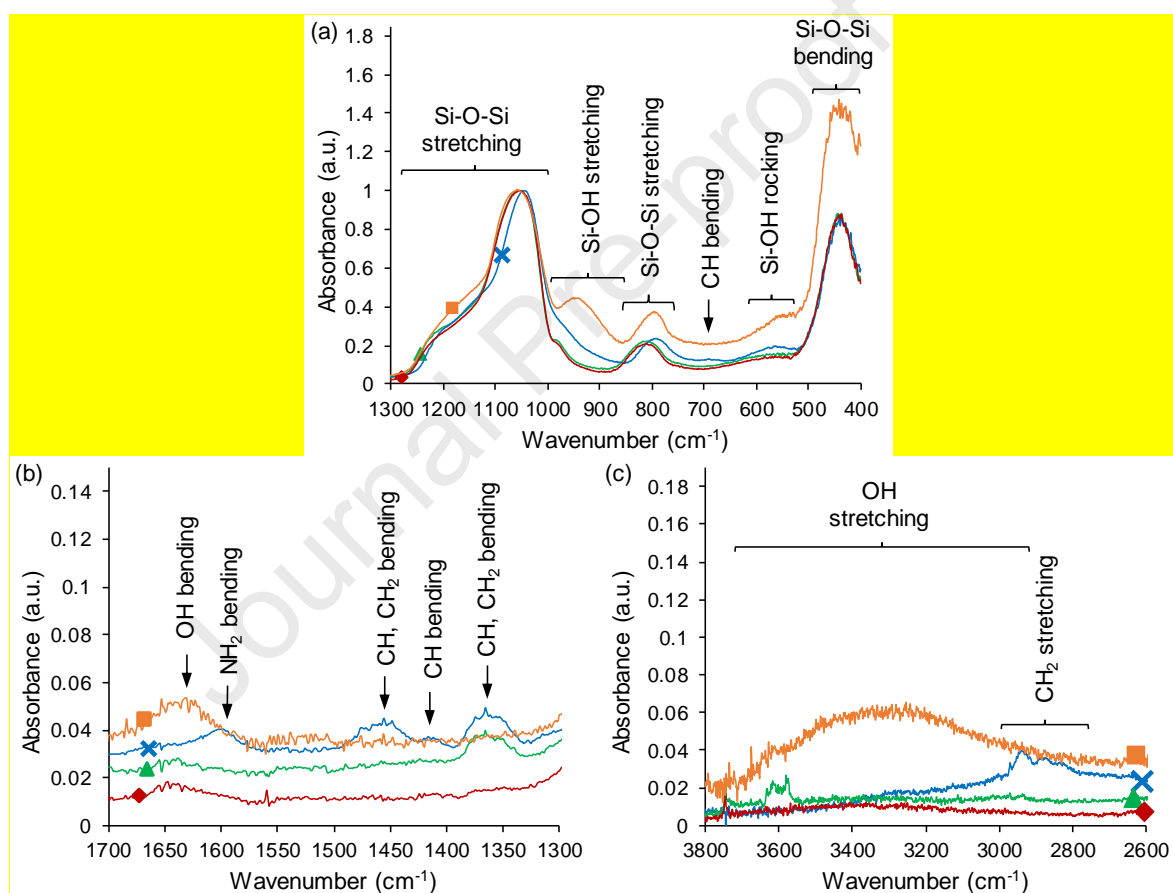
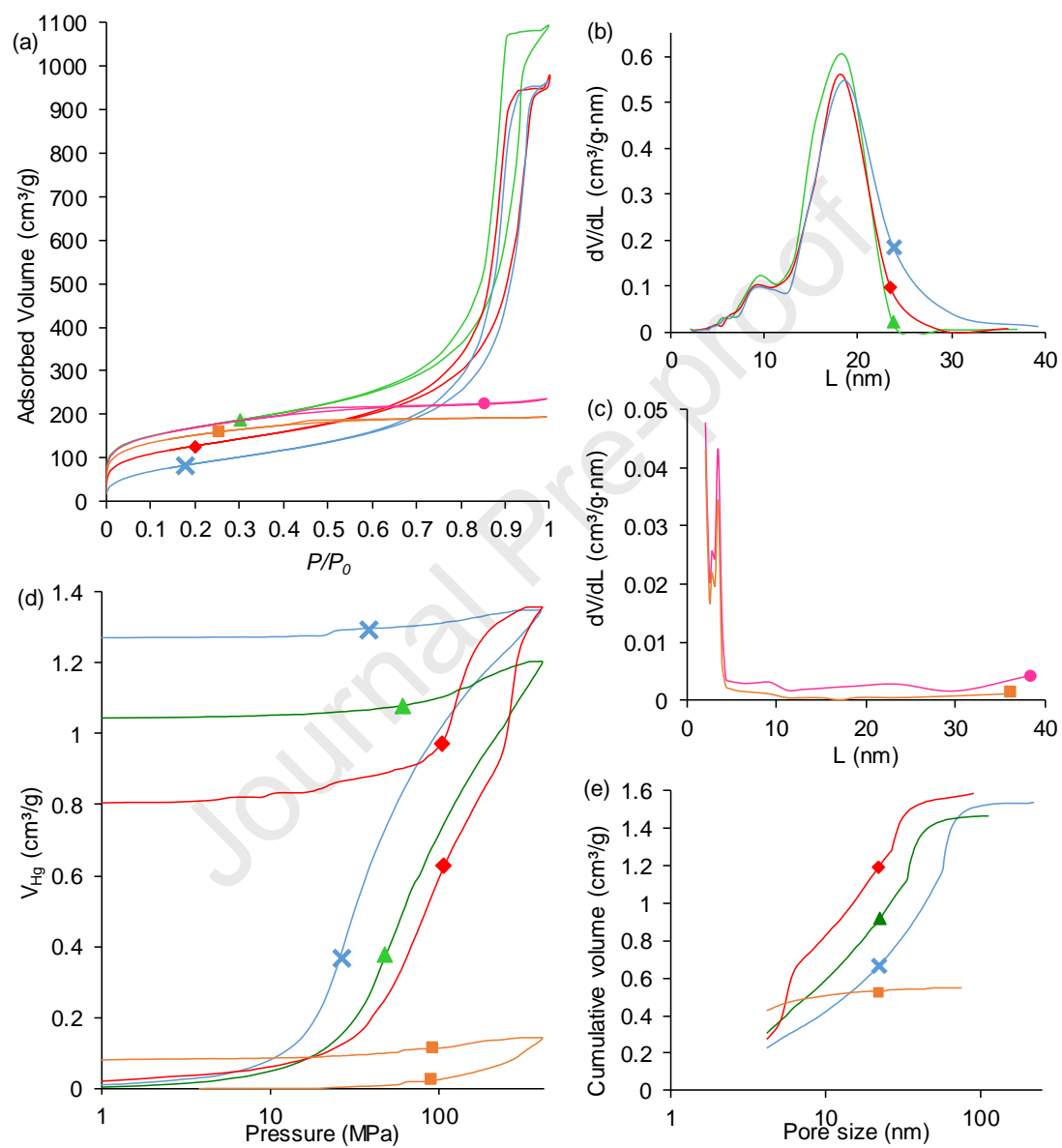
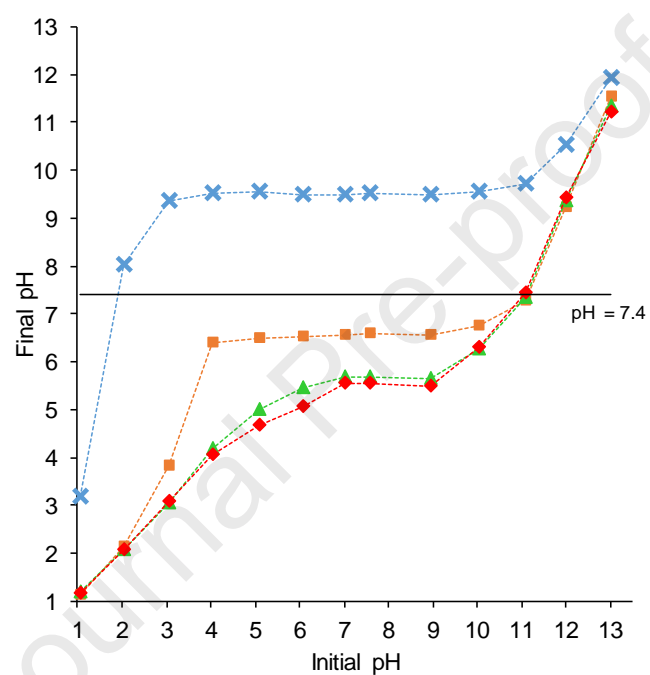
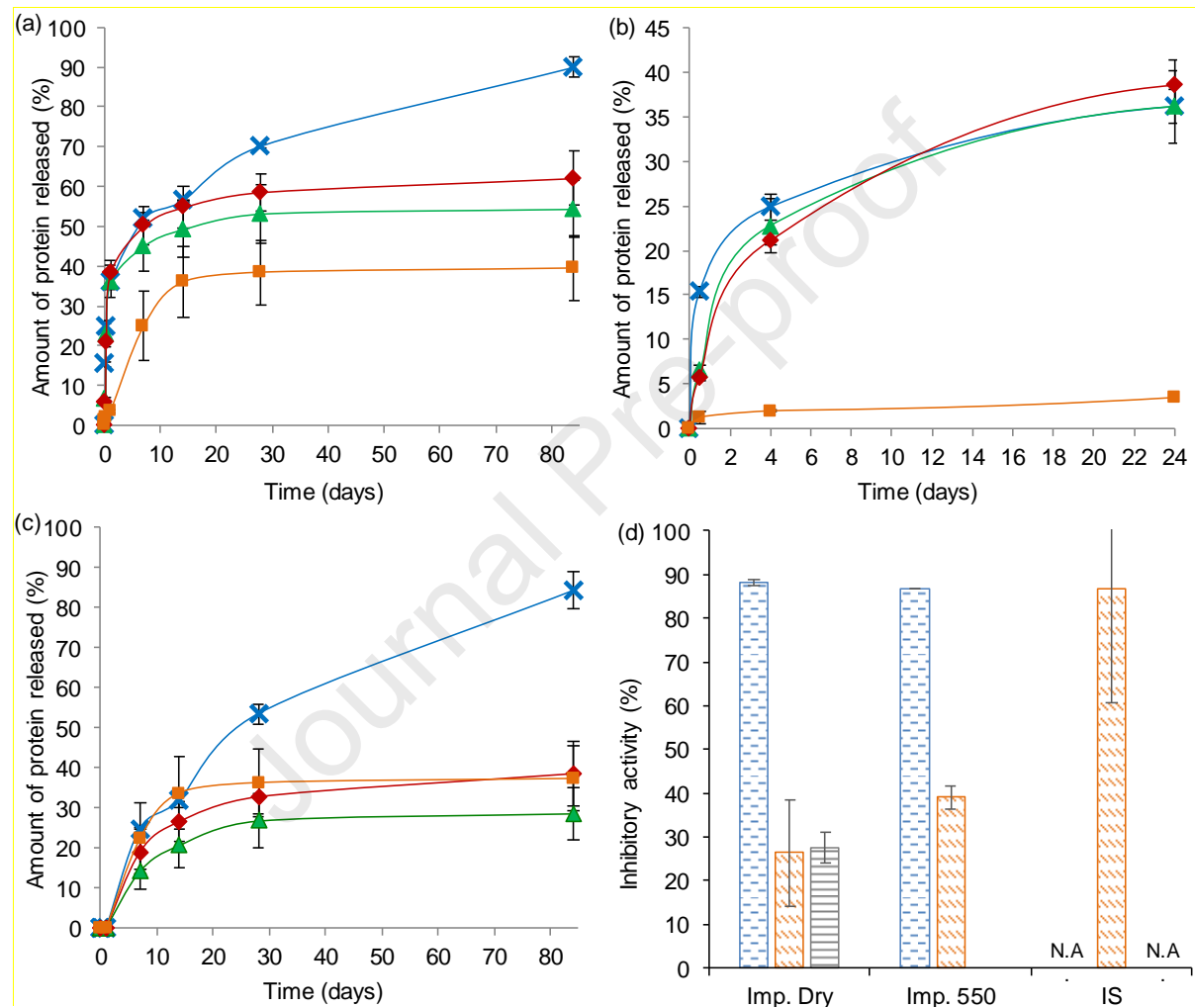
**Figure 1**

Figure 2



**Figure 3**

**Figure 4**



- Encapsulation of STI in functionalized silica via sol-gel process.
- Impregnation method: burst followed by plateau or sustained release.
- Partial or total loss of inhibitory activity for impregnation method.
- *In situ* method: sustained release followed by a plateau.
- No significant change in the activity of the protein for the *in situ* method.

**Declaration of interests**

☒ The authors declare that they have no known competing financial interests or personal relationships that could have appeared to influence the work reported in this paper.

☐ The authors declare the following financial interests/personal relationships which may be considered as potential competing interests: